A time-series of evolving glacial geomorphology for Esjufjallajökull (Breiðamerkurjökull), southeast Iceland

LALLY, Amy, RUFFELL, Alastair, NEWTON, Andrew, STORRAR, Robert <http://orcid.org/0000-0003-4738-0082>, KAHLERT, Thorsten, GRAHAM, Conor, REA, Brice and SPAGNOLO, Matteo

JOURNAL OF MAPS
2025, VOL. 21, NO. 1, 2480798
https://doi.org/10.1080/17445647.2025.2480798

A time-series of evolving glacial geomorphology for Esjufjallajökull (Breiðamerkurjökull), southeast Iceland

Amy Lally [a], Alastair Ruffell [a], Andrew Newton [a], Robert Storrar[b], Thorsten Kahlert[a], Conor Graham[a], Brice Rea[c] and Matteo Spagnolo[c]

[a]School of the Natural Built Environment, Queen's University Belfast, Belfast, UK; [b]Geography, Environment and Planning, Sheffield Hallam University, Sheffield, UK; [c]School of Geoscience, University of Aberdeen, Aberdeen, UK

ABSTRACT

This paper presents four glacial geomorphology maps depicting glacier retreat and landscape evolution between September 2021 and May 2023 at Esjufjallajökull, the central flow unit of Breiðamerkurjökull, southeast Iceland. The foreland, which deglaciated between 2010 and 2023, was mapped from repeat uncrewed aerial vehicle (UAV) survey data. A total of 16 landform types were identified, and their spatial distribution and morphological evolution provide valuable insights into ice and meltwater dynamics during deglaciation. The time-series reveals spatiotemporal variations in landform assemblages: a buried ice environment characterising the western study area, proglacial lakes, hummocky meltwater tracts and eskers dominating the central zone, and meltwater eroded spillways further east. The maps cover an area ranging from 2 to 5.4 km^2, at a scale ranging between 1:4000 and 1:5000.

ARTICLE HISTORY
Received 28 November 2024
Revised 26 February 2025
Accepted 6 March 2025

KEYWORDS
Glacial geomorphology; UAV; temperate glacier; Iceland; Breiðamerkurjökull

1. Introduction

Since the end of the Little Ice Age (LIA), glacial retreat has revealed extensive forelands in Iceland providing ideal locations for investigating the landscape response following deglaciation (Benediktsson et al., 2022; Bennett & Evans, 2012; Chandler et al., 2016a, 2016b; Evans et al., 2010a, 2017c, 2018 ; Everest et al., 2017; Jónsson et al., 2014; Rodríguez-Mena et al., 2021; Schomacker et al., 2014). Geomorphological mapping of these landscapes has significantly advanced our understanding of process-form regimes and interpretation of ancient landforms (Evans et al., 2010b, 2016a; 2016b, 2017a, 2017b, 2023; Evans, 2011; Chandler et al., 2016a, 2020a, 2020b; Lally et al., 2024; Rodríguez-Mena et al., 2021; Schomacker et al., 2014; Śledź et al., 2023). In glacierised settings, the use of uncrewed aerial vehicles (UAVs) is becoming increasingly common due to their ability to produce centimetre-scale digital elevation models (DEMs), at a relatively low cost (Bhardwaj et al., 2016; Chandler et al., 2018; Hackney & Clayton, 2015; Ramsankaran et al., 2020; Śledź et al., 2021).

This paper presents a time-series of four glacial geomorphology maps for the Esjufjallajökull foreland (the central flow unit of Breiðamerkurjökull) depicting ice-margin retreat and landscape evolution over a 20-month period using UAV-derived data. It extends the existing observation period provided by the 1945–2018 time-series of maps (Evans & Twigg, 2000; Guðmundsson & Evans, 2022; Howarth & Welch, 1969a, 1969b) and widens the spatial scope of recent work by Lally et al. (2023, 2024) enabling an evaluation of the rapid ongoing development of glacial landforms at Breiðamerkurjökull during deglaciation at high spatial and temporal resolution.

2. Study area and previous geomorphology research

Breiðamerkurjökull is one of the fastest retreating glaciers on the Vatnajökull ice cap (Aðalgeirsdóttir et al., 2020) which, along with the wealth of historical data on landscape evolution, provides an ideal location for examining landforms uncovered and created during deglaciation. Breiðamerkurjökull comprises four flow units separated by prominent medial moraines (Figure 1). The glacier is underlain by up to 50 m of unconsolidated glaciofluvial sediments on top of fractured igneous bedrock (Boulton et al., 2007a). The glacier has retreated ~7 km in the last 120 years, exposing more than 100 km^2 of foreland (Guðmundsson et al., 2017). Breiðamerkurjökull responds rapidly to the annual cycle of surface air temperatures which previously resulted in annual (winter) push moraine formation (Boulton, 1986;

CONTACT Amy Lally alally01@qub.ac.uk School of the Natural Built Environment, Queen's University Belfast, Belfast BT7 1NN, UK
Supplemental maps for this article can be accessed at https://doi.org/10.1080/17445647.2025.2480798.

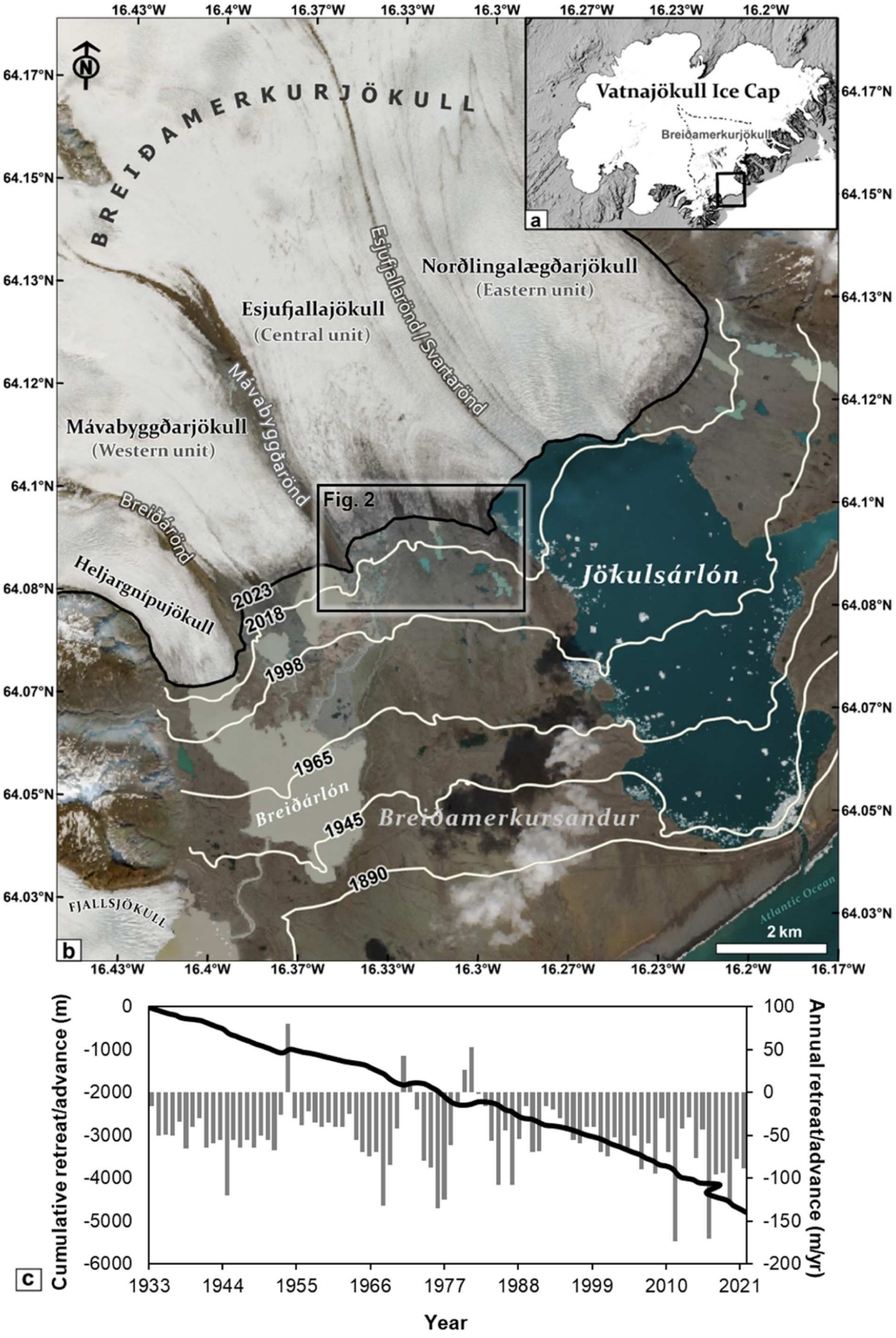

Figure 1. (a) Copernicus EU-DEM hillshade of Iceland and Vatnajökull ice cap. The study area is at Breiðamerkurjökull, an outlet glacier on the south side of Vatnajökull with Figure 1b extent; (b) Breiðamerkurjökull, the four flow units and Breiðamerkursandur. The terminus locations for 1890 and for each year of the previous geomorphology time-series (basemap Sentinel-2 harmonised true colour image 19/09/2023) with Figure 2 extent; (c) Breiðamerkurjökull and cumulative retreat line graph, primary y-axis) and annual retreat rate (bar chart, secondary y-axis) from 1933 to 2022 (data available from https://islenskirjoklar.is).

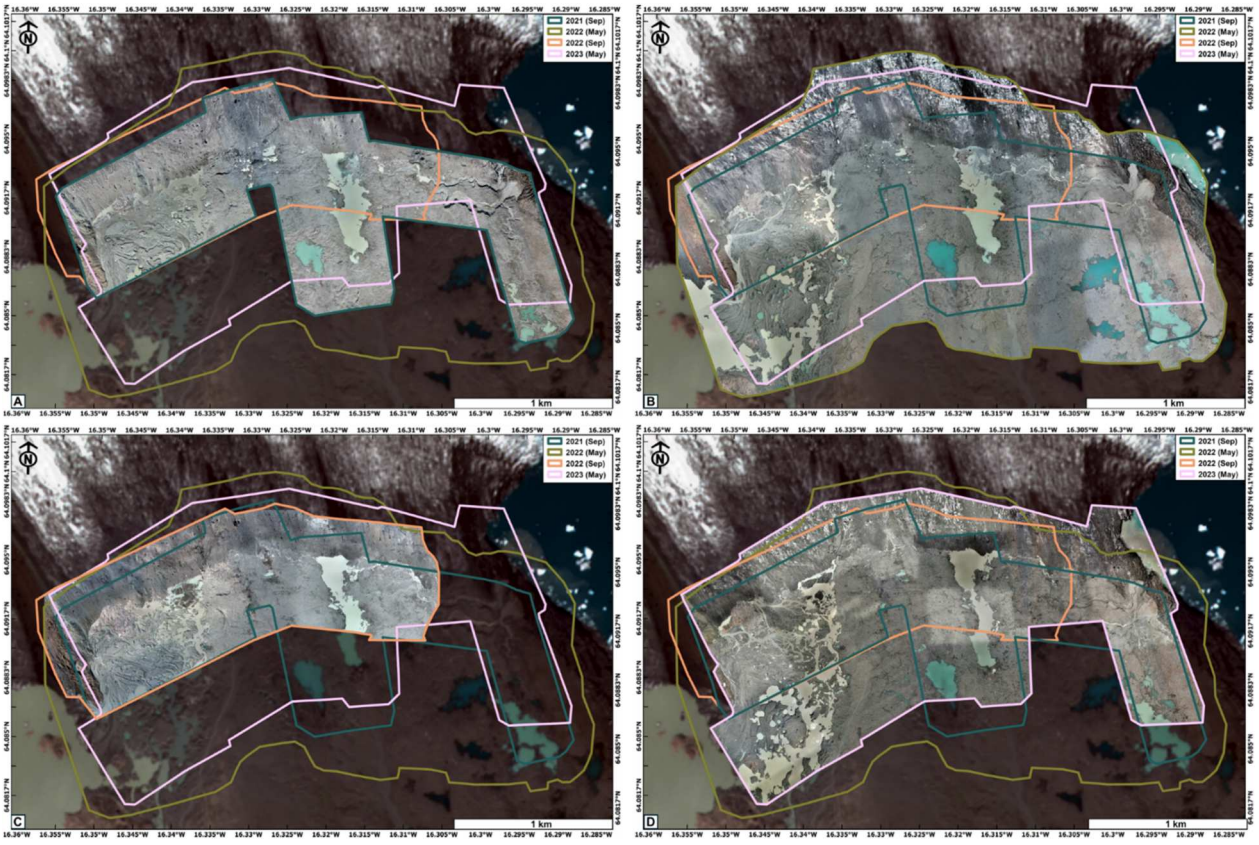

Figure 2. Glacial geomorphology map extents and associated orthomosaic: (a) September 2021 (basemap Sentinel-2 21/09/21), (b) May 2022 (basemap Sentinel-2 06/06/22), (c) September 2022 (basemap 15/09/22) and (d) May 2023 (basemap 01/05/23). The extent of a-d is highlighted on Figure 1b.

Bradwell et al., 2013; Sigbjarnarson, 1970; Sigurdsson et al., 2007).

Breiðamerkurjökull has been the site of seminal research from subglacial deformation experiments (Boulton et al., 2001), the development of process-form regimes (Price, 1969) and the Active Temperate Landsystem Model (Evans & Twigg, 2000). Glacial geomorphology mapping in the area began in the early 1900s, providing a historical record of the glacier's response to climate change (Evans & Twigg, 2002; Howarth & Price, 1969; Lister, 1951; Price, 1969, 1971, 1982; Price & Howarth, 1970). Glacial geomorphology maps were produced for the entire ice-front and foreland for 1945 (Howarth & Welch, 1969a), 1965 (Howarth & Welch, 1969b), 1998 (Evans & Twigg, 2000) and 2018 (Guðmundsson & Evans, 2022). Recent work mapping glacial landforms at Breiðamerkurjökull from UAV data resulted in the refinement of process-form models for englacial eskers (Lally et al., 2023) and ice-marginal spillways (Lally et al., 2024).

The central flow unit (Esjufjallajökull) is the focus of this paper as it is the only predominantly land-terminating section of Breiðamerkurjökull. Many of the other Vatnajökull outlet glaciers (e.g. Kviárjökull, Falljökull, Fjallsjökull Skaftafellsjökull) and the remaining Breiðamerkurjökull flow units currently terminate in proglacial lakes and therefore are unsuitable for mapping landscape evolution from UAV imagery. The 5.4 km^2 study area contains the ice-margin and foreland deglaciated between 2010 and 2023 (Figure 1(b)).

3. Methods and map production

From 2021 to 2023, UAV data were collected during four field campaigns (Table 1). Aerial images were processed in Agisoft Metashape v1.8.1, using structure-from-motion photogrammetry with multi-view stereopsis workflow (Westoby et al., 2012). As ground-truthing improves the reliability of interpretation of later datasets and facilitates ongoing landscape monitoring (Chandler et al., 2018), field mapping and feature verification surveys were undertaken during each field campaign with an additional field verification survey in 6–8 May 2024. Most of the mapped area was surveyed on foot over the five field campaigns. Proglacial channels obstructed access to some western areas of the foreland, additional drone footage was captured here for context to support interpretations. Other areas that were inaccessible for ground control and had ambiguous geomorphology were not mapped including with walls of some erosive features which require further sedimentological work to determine their genesis.

Map production was undertaken using a framework adapted from Chandler et al. (2018) for glacial geomorphological mapping within glacierised settings. Landform

Table 1. Summary of UAV flight and output properties for all four study periods.

	SEP-21	MAY-22	SEP-22	MAY-23
UAV model	DJI Phantom 4 RTK	Two x DJI Phantom 4 RTK	DJI Phantom 4 RTK	DJI Phantom 4 RTK and DJI Mavic 3 RTK
Camera model (focal length)	FC6310R (8.8 mm)	FC6310R (8.8 mm)	FC6310R (8.8 mm)	FC6310R (8.8 mm) FC2403 (4.5 mm)
Flight extent (km^2)	2.80	6.03	2.37	4.71
Flying altitude (m)	105	216	208	109
Number of photos	2735	1327	463	4357
Ground resolution (cm/pix)	2.84	5.86	5.32	2.85
Tie points	619,570	275,190	158,618	1,120,368
Projections	6,282,039	3,064,354	1,090,813	9,665,970
Reprojection error (pix)	0.215	0.175	0.228	0.212
Ground control points	5	4	9	9
Total error (cm/pix)	8.3	2.2	7.2	6.0
Point density (points/m^2)	297	291	353	308
DEM and ortho resolution (cm/pix)	5.8	5.9	5.3	5.7

digitisation and the final map designs were completed using ArcGIS Pro v3.1.1. Features were digitised by analysing a combination of orthomosaics, DEMs, slope-gradient models, traditional and multi-directional oblique weighted (MDOW) Hillshade models. To improve the accuracy of landform digitisation each area had multiple passes (Chandler et al., 2018). To ensure larger features (e.g. meltwater tracts) were accurately delineated the data were viewed at different scales (1:300, 1:1000 and 1:2000). DEMs were overlain onto the Hillshades, using blend modes with Dynamic Range Adjustment activated to ensure variations in elevation were easily visible at each mapping scale. Thousands of field photographs were incorporated into the ArcGIS Pro project using the Geotagged Photos to Points tool for reference throughout the landform interpretation and digitisation process along with the analysis of cloud-free satellite imagery (Planet, Sentinel-2 and Landsat).

The orthomosaics representing the extent of each map are presented on Figure 2. To minimise blank space and enhance aesthetics, each map was produced at a different scale based on the associated UAV survey extent: 1:4500 (September 2021, Main Map 1), 1:5000 (May 2022, Main Map 2), 1:4000 (September 2022, Main Map 3) and 1:5000 (May 2023, Main Map 4) when printed on A1 sheets. The high-resolution versions of the Main Maps are available in the supplementary material.

4. Results

Small-scale reproductions of the map time-series are presented on Figure 3, which includes labels of key areas examined in this paper. The clean high-resolution versions of the Main Maps provided in the supplementary material. Mapped foreland features include large (>300 m diameter) homogenous areas of streamlined subglacial material (i.e. till) to individual kettle holes less than 1 m in diameter (Figure 4).

4.1. Glacial and stagnant ice

The active ice margin was delineated based on topographic variations and colour on the orthomosaic. The glacier terminus was either gently sloping onto the foreland or formed ice-cliffs if undercut by meltwater. Mapped glacial ice ranged from 23-35% of the total area within each map and retreated up to 196 m throughout the time-series in response to deglaciation. Ice blocks, detached from the main glacier margin, and areas of glacial ice partially submerged by water visible on the orthomosaics, were mapped as separate features termed 'stagnant ice'. Buried ice was observed beneath pitted glaciofluvial deposits in the foreland and was not digitised as an individual feature.

4.2. Medial moraine

Medial moraines are positive relief ridges separating ice flow units, brown in colour, ice-cored and contain angular boulders. The Mavabyggdarönd medial moraine was mapped in the west and the Esjufjallarönd medial moraine in the east. Medial moraines constitute 2-6% of each map. The eastern foreland area, once the location of the medial moraine, had a spread of large angular boulders left behind as the medial moraine downwasted. It was difficult to accurately delineate where the boulder spread began and ended and large boulders were observed at multiple locations across the foreland. Therefore, these boulder fields were not mapped as a separate feature. The study area was classified based on the dominant geomorphology (e.g. hummocky meltwater tracts or till). However, as stated by Evans and Twigg (2002), these boulder deposits are linked to the ample availability of supraglacial debris (i.e. from medial moraines or supraglacial debris stripes).

4.3. Bedrock areas

Bedrock was primarily mapped at the western ice-margin with isolated outcrops (<2 m wide) along the floor of a meltwater eroded spillway in the east. Bedrock areas were split into two distinct features, the first was bedrock outcrops or exposures, often polished and striated. The second was mapped as

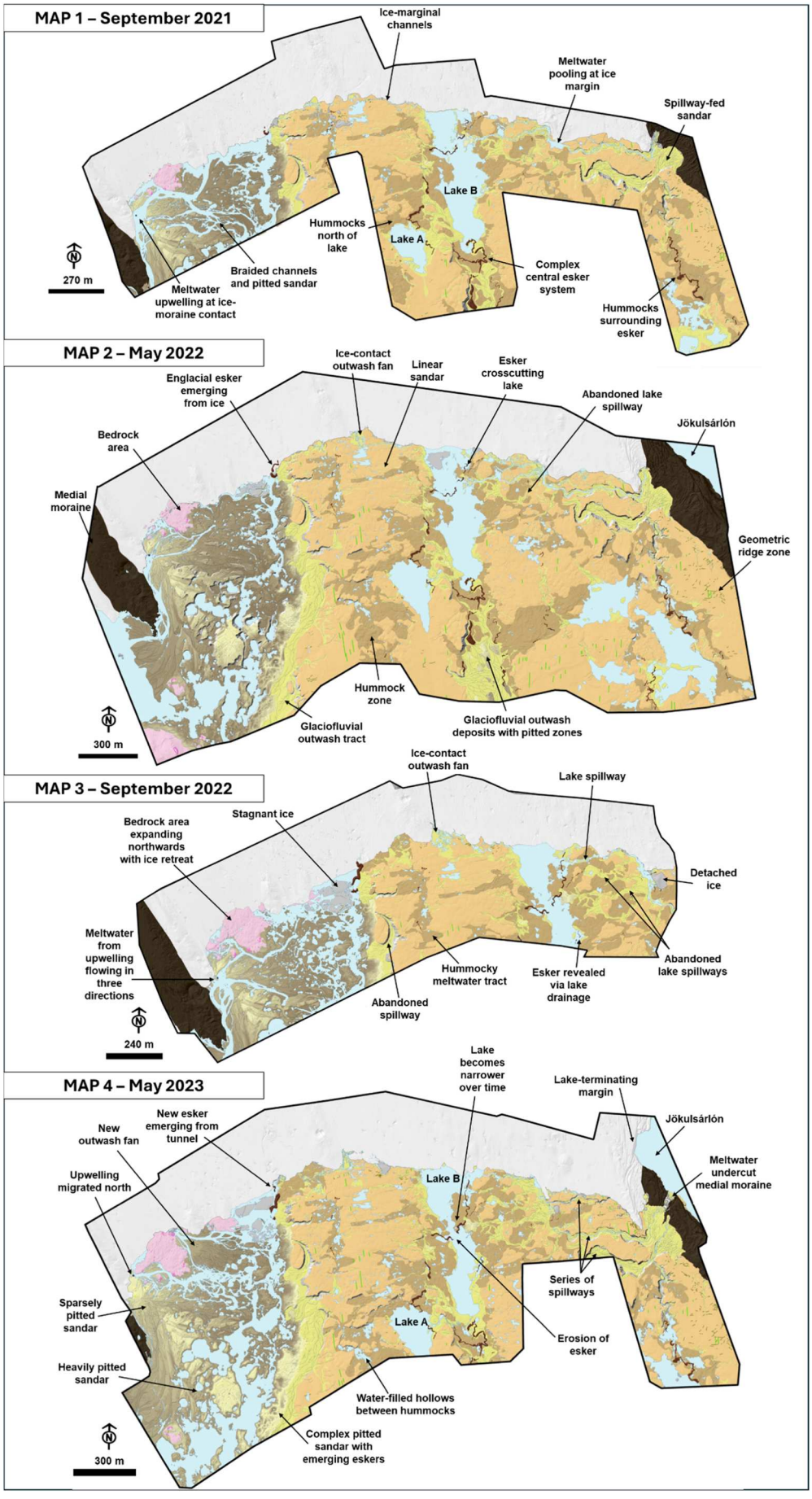

Figure 3. The four-map glacial geomorphology time-series representing Main Map 1 (September 2021), Main Map 2 (May 2022), Main Map 3 (September 2022) and Main Map 4 (May 2023). The high-resolution versions are available in the supplementary files.

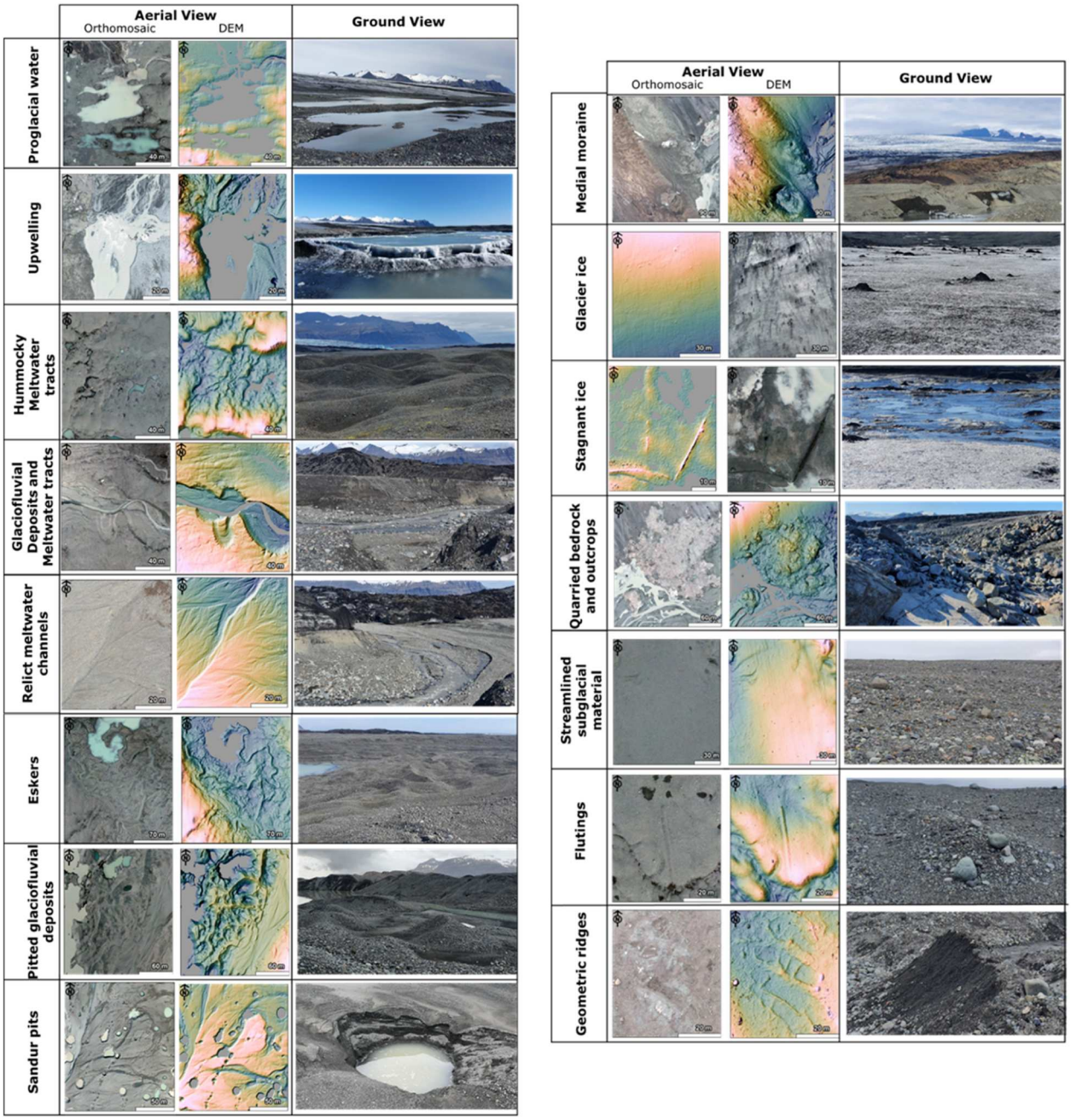

Figure 4. Aerial view of the mapped features (DEM and orthomosaic) with an example of the indicative ground view from field photos. The DEM is underlain by an azimuth 315° Hillshade, Dynamic Range Activated so each DEM elevation ranges from the lowest (blue), intermediate (green yellow) to highest (pink), the areas of proglacial water are masked (grey).

areas of 'quarried bedrock' which contain angular blocks to large boulders (> 1 m in diameter) often overlying outcrops. The bedrock at the western ice-margin is likely the northeast continuation of the bedrock highpoint fronting the western flow unit (Mávabyggðarjökull) (Guðmundsson & Evans, 2022) which can be seen in the bottom left corner of the May 2022 geomorphology map (Main Map 2 in the supplementary material). Bedrock areas ranged from 0.5-2% of the total area on each map.

4.4. Streamlined subglacial material

Streamlined subglacial material, also termed ground moraine, till and fluted till (Evans & Twigg, 2002; Guðmundsson & Evans, 2022), is the most common foreland feature mapped (16–26% of total map area). Streamlining was visible on the DEMs across broad areas but digitising individual bedforms was challenging due to their subtle topographic expression. The subglacial material across the Esjufjallajökull foreland is composed of unconsolidated sediments and overridden features deposited during previous ice advances (Evans & Twigg, 2002; Guðmundsson & Evans, 2022). The streamlined terrain occupies the highest elevations across the foreland, represent the former subglacial bed and are often flanked by meltwater tracts and proglacial lakes. Zones of streamlined subglacial material in the foreland are unmodified throughout the time-series and are absent in the western area of each map.

4.5. Flutings

Flutings, elongated low relief ridges and furrows (<0.5 m high), record previous ice flow directions (Figure 5). Up to 80 flutes were digitised in each map with lengths ranging between 8-80 m. Their azimuth ranges between 165° (SSE) and 189° (SSW) with a south mean direction (178°). Lodged boulders were often located at the initiation point, with the flutings likely formed by till squeezing into cavities on the downglacier side of these boulders (Benn, 1995; Boulton, 1976; Evans & Twigg, 2002). Flutings were disrupted by hummocks in some locations (Figure 5(b,c)), suggesting they formed earlier.

4.6. Geometric ridges

Geometric ridges, which are low relief linear features (<0.5 m high), represent previous ice fracture or basal crevasse locations, often forming reticulated networks and are closely associated with streamlined subglacial material (Figure 5(d)). Further work is required to determine the genesis of these features (i.e. crevasse-squeeze ridges, hydrofractures infills or surface crevasse infills), therefore, they have been mapped as 'geometric ridges' after Evans et al. (2022) who identified similar features in Svalbard. Ridge lengths are between 1–37 m, with an average of 8 m. Although ridges occur in multiple orientations, the average bearing is 89° (i.e. E-W and perpendicular to ice flow). These ridges were primarily identified in the eastern part of the study area, the Esjufjallarönd medial moraine zone. Similar features were also mapped in 2018 to the area east of Jökulsárlón by Guðmundsson and Evans (2022).

4.7. Proglacial water

Meltwater covered 12-17% of the mapped area, including proglacial lakes, ice-marginal channels,

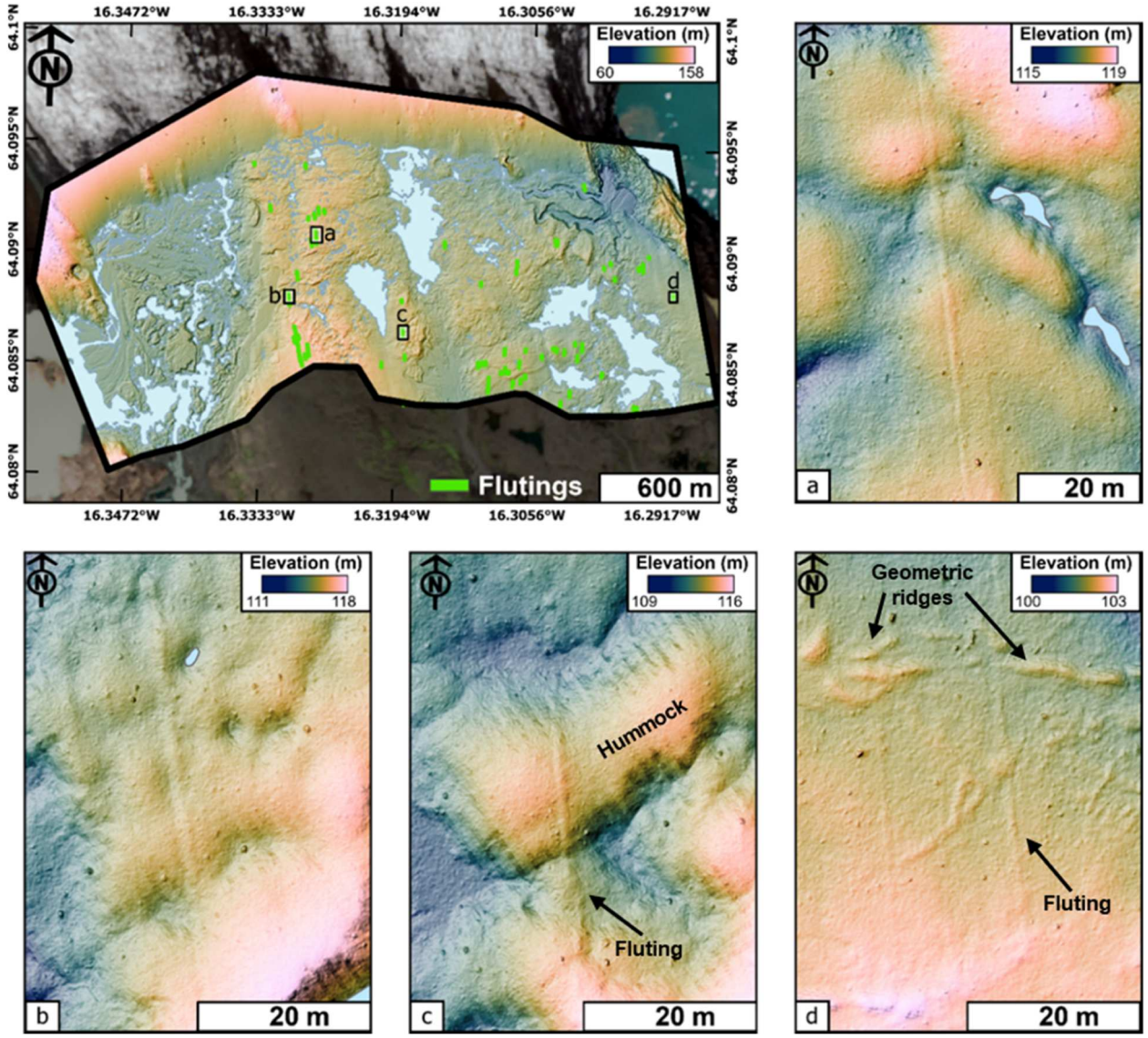

Figure 5. The spatial distribution of flutings in May 2022 and four zoomed in examples: (a–c) flutes on streamlined subglacial material or edge of hummocky zones; (d) flutes on subglacial material on the east, cross-cut by geometric ridges (May 2022 DEM and Hillshade model basemap [note in Figure 5b-c the NW-SE gridded pattern is a UAV-processing artefact].

water-filled pits and pools between hummocks. The topography prevents free drainage of meltwater away from the ice-margin resulting in submersion of snoutice or meltwater drainage concentrated along the glacier terminus (rather than flowing away from it). The hollows between hummocks across the study area are filled with ephemeral lakes, which drain over time and often re-fill during the winter months, as observed by the increased presence of water in the May maps compared to the September maps. This may be due to higher precipitation over the winter months or groundwater recharge.

The centre of the study area is dominated by two lakes. Proglacial Lake A, which was disconnected from the active ice-margin in ~2014, had a maximum area of 42,483 m^2. Proglacial, and still ice-contact in 2023, Lake B expanded northwards with the ice-margin and narrows throughout the time-series reaching a maximum area of 119,184 m^2. Lake B drains eastwards through a series of spillways, which progressively become abandoned as the glacier retreats. These spillways were examined by Lally et al. (2024) and form in response to the glacier retreating across a reverse-slope bed and the impoundment of water at the ice-margin.

One meltwater upwelling was identified on each map. The upwelling was always observed and mapped next to the western medial moraine, similar to the upwelling at Skaftafellsjökull observed by Tweed et al. (2005). Meltwater upwellings are most common near major subglacial meltwater sources and form by drainage from high pressure to lower pressure regions (Boulton et al., 2007a, 2007b). The emerging meltwater was likely supercooled as it flows from a subglacial artesian vent, evidenced by the formation of frazil and anchor ice around fine-grained terrace deposits (Figure 6). In the final map of the series (May 2023), the zone of upwelling migrated 125 m north from the 2021–2022 location.

4.8. Glaciofluvial outwash deposits and meltwater tracts

Glaciofluvial features, representing 6–9% of each map area, include erosional (i.e. meltwater tracts) and depositional features (i.e. glaciofluvial outwash). These features include ice-contact and spillway fed outwash fans, meltwater eroded spillways (>5 m wide) and narrower meltwater channels (<2 m wide) eroded into subglacial sediments. Up to 1,247 relict or abandoned meltwater channels, ranging in length from 2 to 700 m, were digitised as line features on each map. These were concentrated across the braided outwash fans, highlighting the spatiotemporal variation in meltwater flow directions. Time-transgressive series of glaciofluvial outwash tracts (Lake B outflow spillways) provide evidence for channel incision and abandonment in response to ice retreat and emerging topography (Evans & Twigg, 2002; Lally et al., 2024).

Small patches of fine-grained deposits were mapped surrounding Lake A and B, as well as on the till and between hummocks. Although these areas often had weakly developed shorelines, they were not mapped as separate features because later meltwater flow often disturbed them, making it challenging to distinguish sediments deposited in lakes from those in streams.

4.9. Pitted glaciofluvial deposits

The western part of the study area, along with isolated regions associated with the central ice-contact proglacial lake, contain glaciofluvial outwash fans with pitted surfaces that account for 9-15% of each map's area (Figure 7). Pitted outwash is linked to the melting of buried glacier ice at retreating temperate glacier margins (Guðmundsson & Evans, 2022). In earlier maps (e.g. Evans & Twigg, 2002; Howarth & Welch, 1969b) pitted sandar was termed 'kame and kettle topography' but has since been more appropriately termed 'kettled' or 'pitted sandar' (Guðmundsson & Evans, 2022).

Pitted sandar fans reach widths of 55 m in the western area and up to 15 m in the central foreland. The time-series captures the creation of terraces in these areas, eroded by later meltwater flow. Buried ice is visible in the walls of the pits up to 850 m from the active western ice margin (Figure 7(e)). Pits are predominantly quasi-circular depressions in the surface of flat glaciofluvial outwash deposits and can be water-filled due to a high-water table or impermeable surfaces at the base of the pit. The ~6 cm resolution orthomosaics and DEMs allowed for the digitisation of individual pits as point features and up to 1,738 pits were digitised for each temporal snapshot. Flat glaciofluvial outwash deposits with sparce pitting (Figure 7(a)) were mapped closest to the active glacier which evolved into sandar with enlarged pits further from the active ice-margin (Figure 7(b)). The glaciofluvial deposits overlying the buried ice collapse over time or are eroded by later meltwater flow (Figure 7(c)). The most complex sandar was observed furthest from the ice-margin with esker ridges emerging from the sandar as buried ice surrounding the ridges melts over time (Figure 7(d)). Ridges emerging from the sandar were commonly straight (Boulton et al., 2007a; Storrar et al., 2015).

In line with previous work (c.f., Guðmundsson & Evans 2022; Howarth, 1971; Price, 1982; Welch & Howarth, 1968) pitted sandar and emerging eskers represent various stages on a process-form continuum and should not be genetically separated. However, to better visualise the complex topography in the geomorphology maps a colour gradient was used across

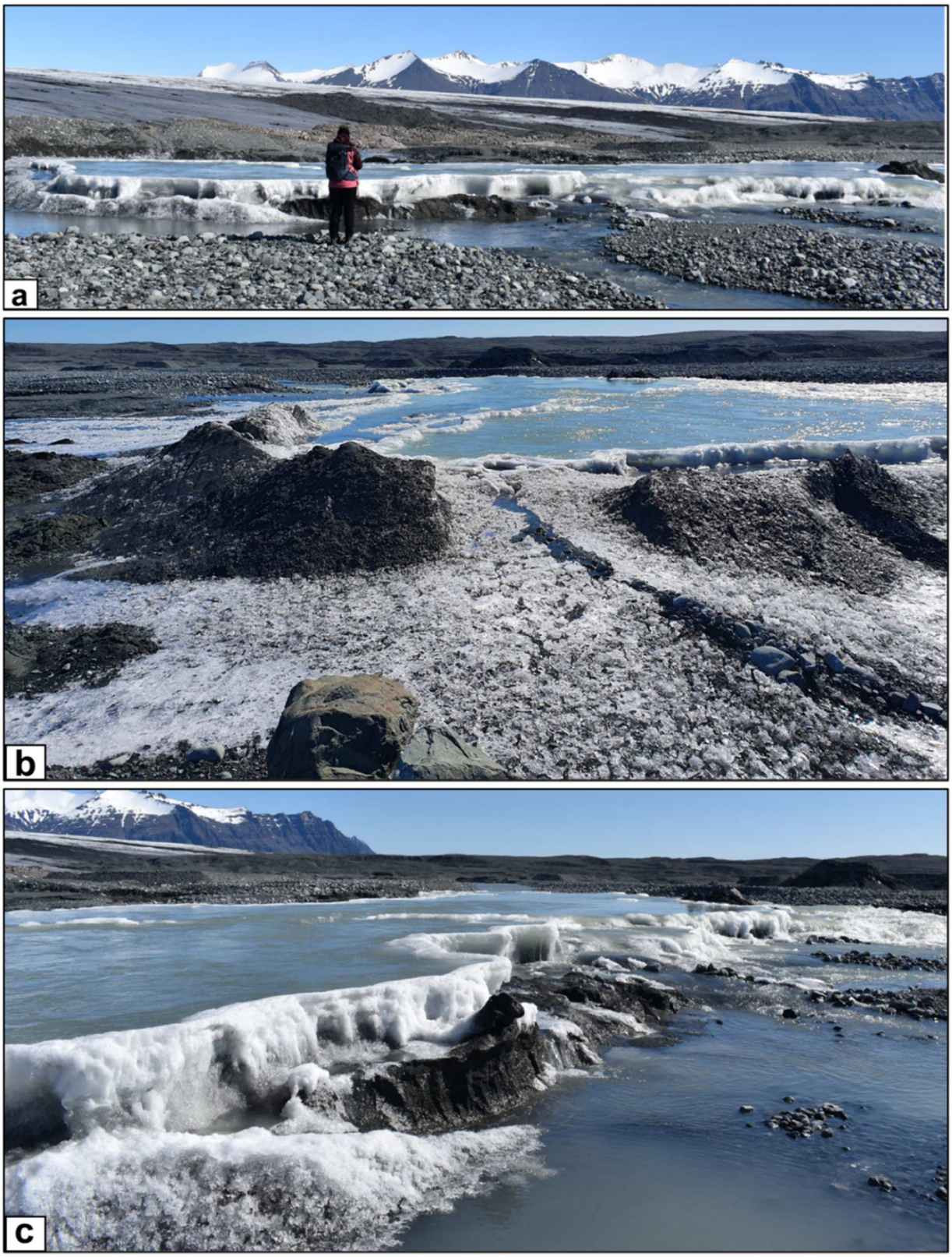

Figure 6. Field photos of the meltwater upwelling near the western ice-margin in May 2022: (a) the meltwater upwelling and the terrace deposits (photo looking northwest); (b) frazil ice surrounding the upwelling providing evidence for supercooling (photo facing west) and (c) terrace deposits and frazil ice (~40 cm high) surrounding the meltwater upwelling (photo facing west).

the pitted sandar areas. High elevation areas are shown in yellow, representing emerging eskers further south and newly deposited outwash in the north (Figure 3). Lower elevation areas with collapsing pitted surface were coloured brown. This colour gradient allows for better visualisation of the complex topography. Only esker ridges outside of pitted sandar deposits were mapped as individual features.

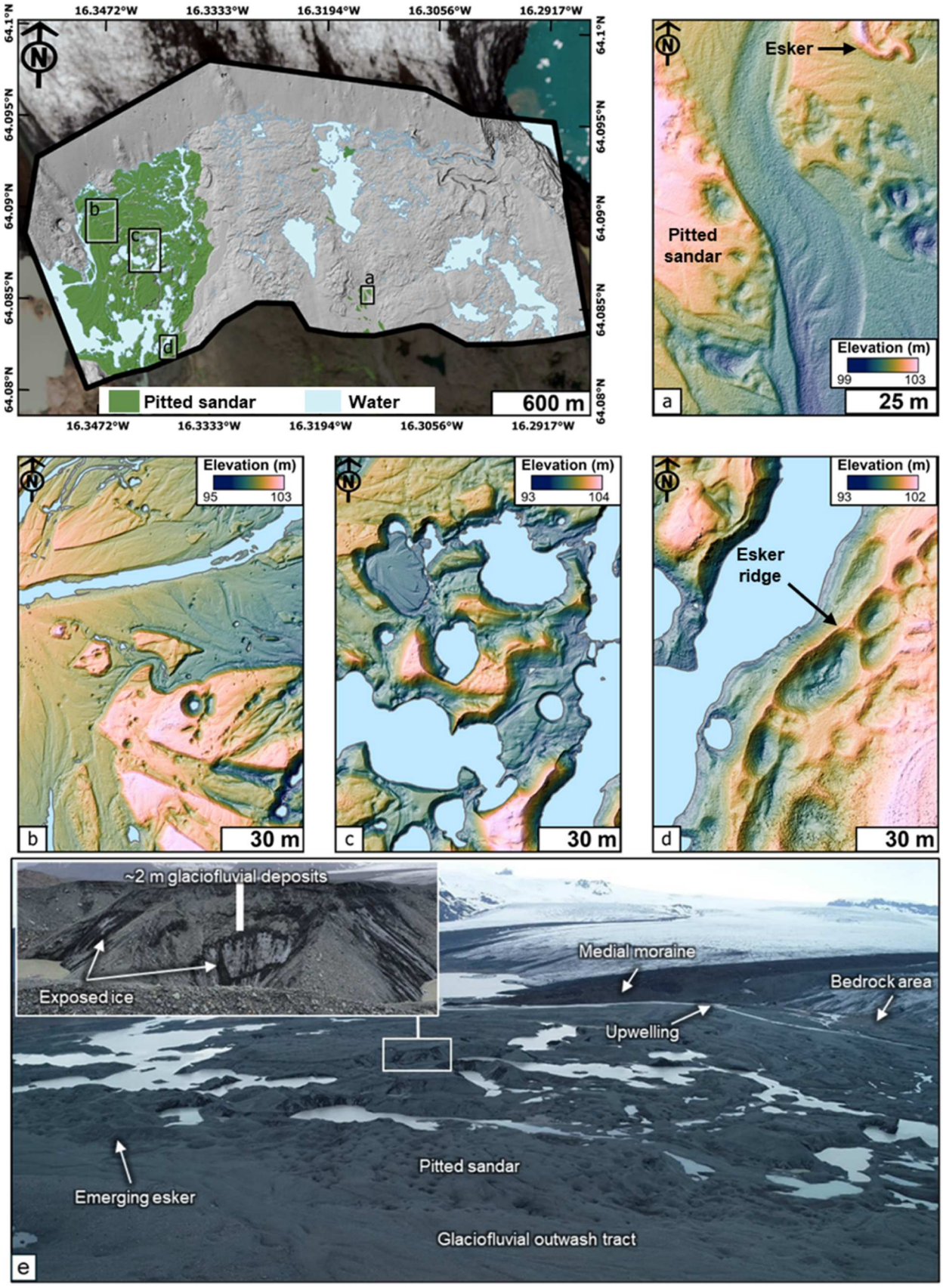

Figure 7. Distribution of pitted sandar across the study area, with insets of different phases of evolution (May 2022 Hillshade model basemap): (a) pitted sandar fans cross-cut by braided outwash; (b) flat braided outwash with small pits and a terraced pitted sandur fan; (c) terraced pitted sandar to adjoining water-filled pits; (d) complex pitted sandar with an emerging esker. Water-filled areas are in solid blue polygons (May 2022 DEM basemap); (e) UAV photo of pitted sandar area (photo facing west) with field photo inset highlighting buried ice in foreland (photo facing west).

4.10. Hummocky meltwater tracts

Hummocky meltwater tracts account for 9-13% of each map (Figure 8). These are areas consisting of irregular mounded terrain, often mapped between areas of streamlined subglacial material at lower elevations, like those mapped by Öhrling et al. (2020). The hollows between the hummocks often contained fine-grained glaciofluvial/lacustrine deposits and ephemeral lakes which dry up over the summer months. Hummocks and the intervening hollows were mapped as the same feature. They were delineated based on the dominant geomorphology and whether a tract consisted mostly of hummocks.

Hollows between hummocks cross-cut and disrupted flutings indicating they may have formed later (e.g. Figure 5(c)). This provides evidence, along with topographic differences between the fluted till and hummocky topography that these hummock corridors are likely modified, at least in part, by meltwater erosion. Perhaps these areas represent reworking of sediment by proglacial water, evidence for high subglacial meltwater supply to the base of the ice and a weakly connected cavity system (i.e. hollows between the hummocks) (Ahokangas et al., 2021; Leigh et al., 2021; Öhrling et al., 2020; Ojala et al., 2019; Peterson et al., 2017).

Some of the hummocks, particularly in the area surrounding Lake A, appear to have a consistent orientation (NNW-SSE similar to the ice flow direction) similar to triangular-shaped hummocks (Figure 8(a–c)) termed 'Murtoos' mapped across the former bed of the Scandinavian Ice Sheets (SIS) (c.f., Ojala et al., 2021). Although the Breiðamerkurjökull hummocks do not have a well-developed V-shape like the SIS examples, some areas do resemble lobate type murtoos classified by Ojala et al. (2021). The spatial distribution of these hummocky tracts supports this interpretation as they are primarily found in zones between streamlined subglacial material and potential major meltwater sources containing eskers and proglacial lakes. These hummocky areas could provide evidence of a transitional drainage system between efficient and inefficient although further work is required to improve our understanding of the associated process-form regimes.

4.11. Eskers

Eskers are straight-to-sinuous ridges comprising glaciofluvial sand and gravel (Banerjee & McDonald, 1975), with their footprints delineated based on break of slope. Up to 30 eskers were identified on each map, accounting for <1% of each map, ranged from <10 m to 560 m in length (Figure 8). The evolution of an englacial esker emerging from the ice-margin (Figure 9), examined by Lally et al. (2023), was captured in the first three maps of the series. Further evolution of this feature, and the emergence of another englacial esker, can be seen in the final map (May 2023).

Storrar et al. (2015) concluded that the formation of eskers' is controlled by both sediment supply and meltwater availability, with the largest eskers found at the medial moraine locations. The spatial distribution of the eskers across the mapped area indicates stable meltwater sources existed in the central foreland (Lake A and B) and in the eastern foreland enabling their deposition in perennial channels (Boulton et al., 2007a). Smaller eskers may provide evidence for deposition in transient channels created during individual meltwater seasons.

4.12. Landscape evolution over the study period

An area of 0.44 km^2 was deglaciated between the September 2021 to May 2023 ice-margin locations, 24% of which exposed streamlined subglacial surfaces. Water-submerged topography replaced 24% of the retreating ice margin, mostly associated with the western ice-margin and the central lake (Lake B). Hummocky meltwater tracts occupied 15% of the deglaciated terrain, glaciofluvial deposits 14% and pitted sandar 10%. Bedrock exposures replaced 9% of this area, stagnant ice 4% and eskers <1%. Evolution of the proglacial landscape, already exposed in the first map of the series, in response to post-depositional processes was also captured in the maps (e.g. Figure 9). This includes the erosion of eskers by later meltwater flow and pit enlargement due to buried ice melt out. The bedrock zone extended over 100 m north over the study period with a x2.5 increase in area (Figure 9). Areas of streamlined subglacial material and hummocky meltwater tracts remained static and unchanged across the time-series unlike the evolution observed across the pitted sandar.

4.13. Comparison with existing time-series of Breiðamerkurjökull maps

Although the 2018 map of Breiðamerkursandur, by Guðmundsson and Evans (2022), covers the entire ice-margin of Breiðamerkurjökull, the foreland of the central flow unit (Esjufjallajökull) can be compared against the landform assemblage presented in this paper. The bedrock outcrop to the south of the Mávabyggðarönd medial moraine, on the 2018 map is visible on the southwest of the May 2022 map. Kame and kettle topography, termed 'pitted glaciofluvial deposits' in this work, was noted at the ice-margin which was also mapped in our work but extends over 300 m further north by 2021. The relict meltwater channel tract running alongside the pitted sandar

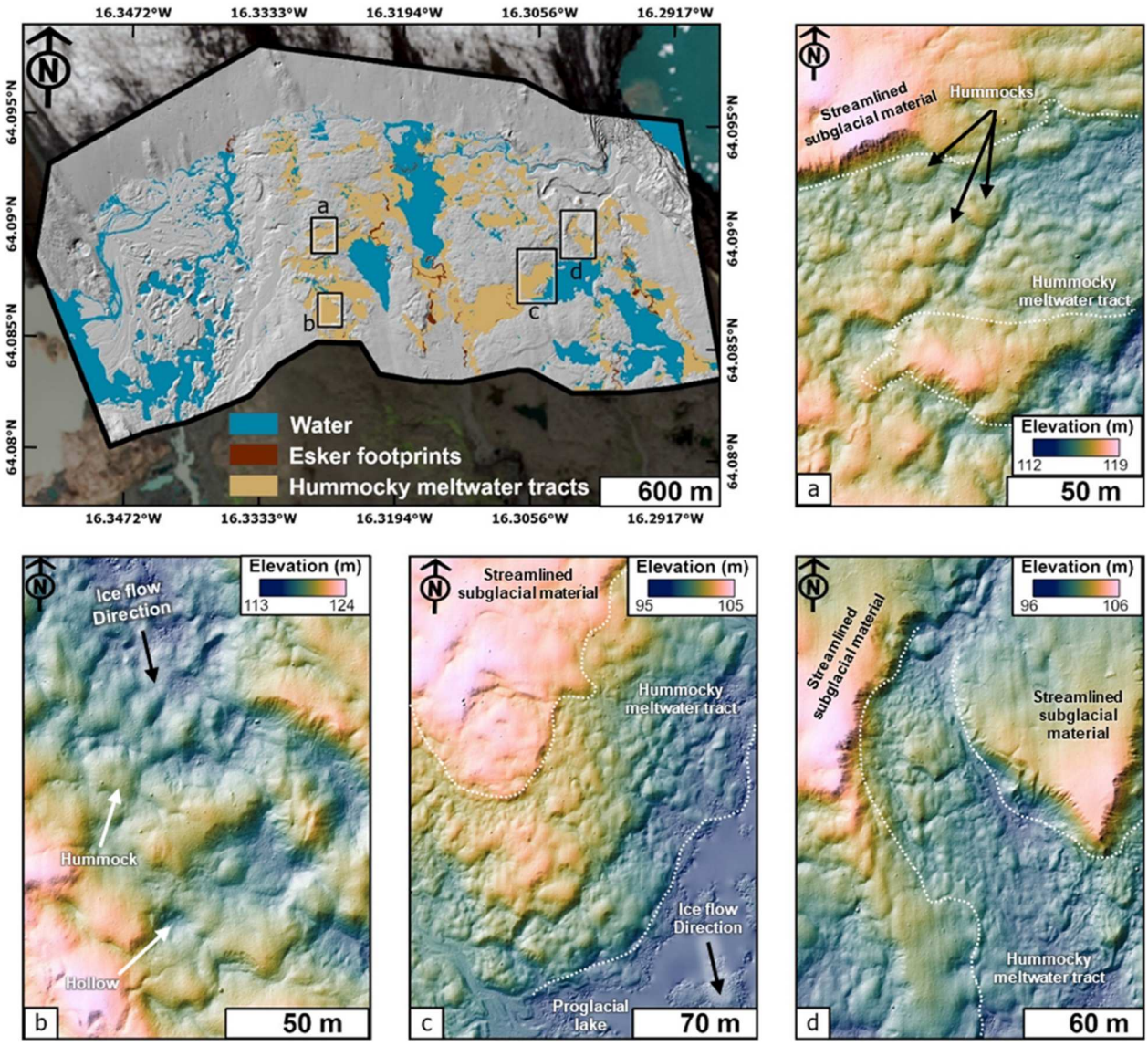

Figure 8. Hummocky meltwater tract distribution, and associated water and eskers, across study area (top, traditional hillshade model basemap) with four examples of morphology with the tracts outlined with the white dotted lines (DEM and Hillshade model basemap).

and the streamlined subglacial material to the east is also depicted on the 2018 map. Proglacial lakes in this area are no longer present but are replaced by hummocky meltwater tracts. The remainder of the ice-margin is dominated by fluted till in the 2018 map, termed 'streamlined subglacial material' in our time-series.

The hummock zone west of Lake A was mapped as 'hummocky moraine' in the 2018 map. Hummocky moraine is associated with the melt-out of medial moraines, providing evidence for sufficient amount of supraglacial sediments to create chaotic hummocky terrain as the glacier downwastes and retreats (Evans & Twigg, 2002). This area was mapped as 'hummocky meltwater tract' in this time-series as the hummocks in this area were like those observed to the east of Lake B. As hummocks disrupt flutings and appear to have a preferred orientation to ice flow in some areas, we suggest these may represent zones of enhanced meltwater flow which removes sediment around the hummocks, rather than the hummocks being deposited by supraglacial debris meltout. Further work is required, including sedimentological and geophysical investigations, to understand the development of these hummocky areas which may involve multiple processes.

The historical evolution of Breiðamerkurjökull eskers is well-documented (Evans & Twigg, 2002; Howarth, 1971; Price, 1969, 1973, 1982; Storrar et al., 2015). Previous mapping efforts at Breiðamerkurjökull indicate eskers between Breiðárlón and Jökulsárlón are over 2 km in length (Evans & Twigg, 2002; Storrar et al., 2015). Eskers mapped in this time-series were shorter, with a maximum length of 560 m and were not captured in the 2018 map, likely due to their narrow morphology (e.g. maximum width of ~4 m), which highlights the value of using high-resolution UAV imagery. Complex esker systems

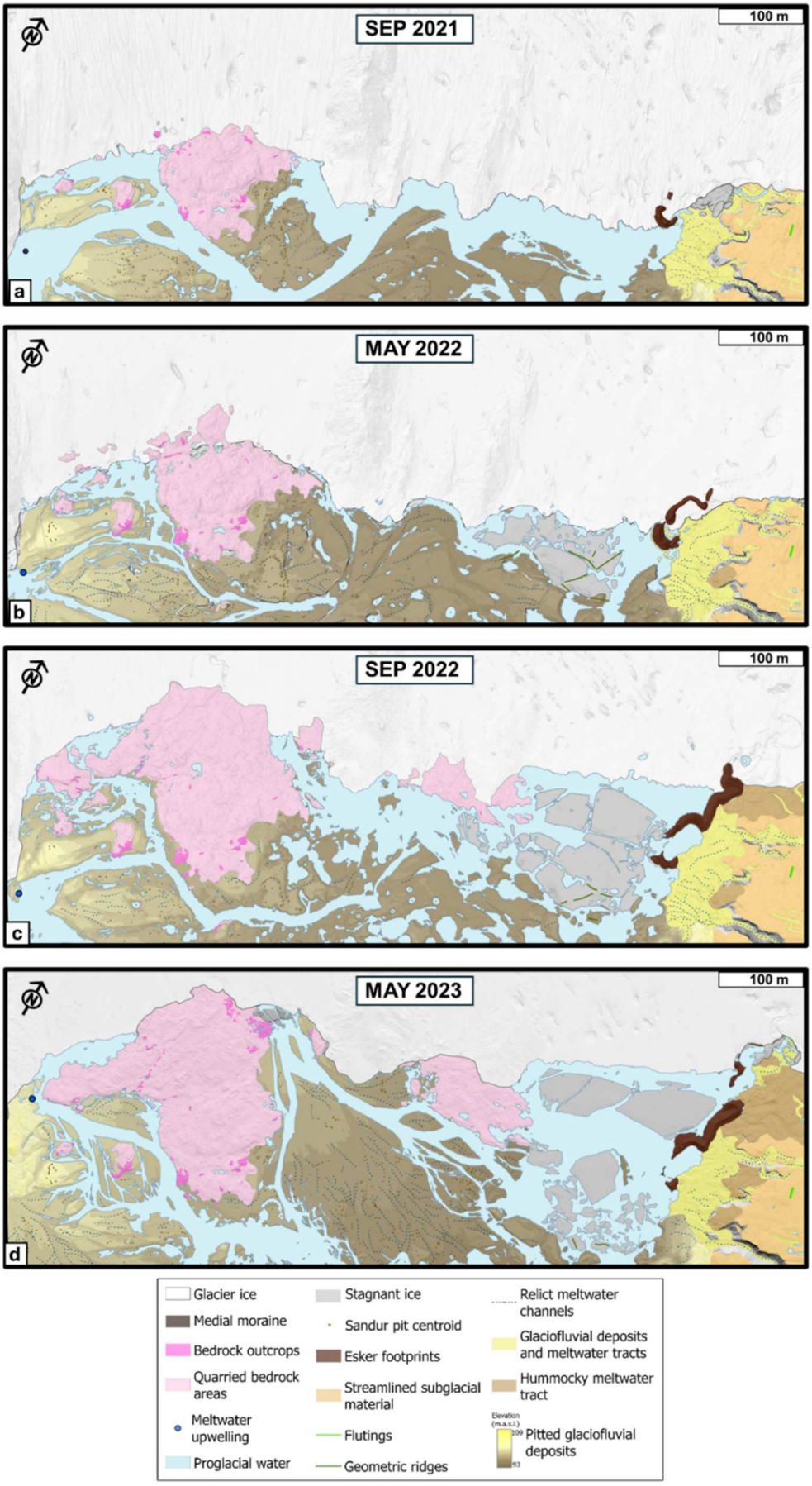

Figure 9. Inset of the western ice-margin for all four maps (a) in September 2022; (b) May 2022 highlights changes in the width and location of proglacial channels compared to the previous map and the englacial esker is observed melting from the ice-margin; (c) by September 2023 pitting becomes more developed across the pitted sandar area and the bedrock area extends to the north; (d) by May 2023 a new meltwater source east of the bedrock area deposits a new outwash fan that will likely become pitted over time as buried ice melts out.

can gradually emerge from terraced pitted outwash deposits as buried ice-melts out over time (Evans & Twigg, 2002; Howarth & Price, 1969; Howarth, 1971; Storrar et al., 2015; Welch & Howarth, 1968). From the Hillshade model beneath the 2018 map, it is clear to see the evolution of the pitted sandar over the following four years, which enlargement of pits and the formation of terraced pitted deposits by later meltwater flow by 2021.

5. Discussion and conclusion

Four geomorphology maps are presented in this work providing a time-series of proglacial landscape evolution at Esjufjallajökull (the central flow unit of Breiðamerkurjökull) from September 2021 to May 2023. These maps highlight the value of using UAVs for mapping dynamic environments as the use of high-resolution DEMs enables the identification of features that are not obvious from satellite, UAV-derived orthomosaics or even from ground view (e.g. eskers, hummocky areas, pits and relict meltwater channels).

The spatiotemporal variation in landform assemblages corresponds to the evolving topography. The subglacial topographic setting, from Björnsson (1996), can be summarised as a higher elevation central region (i.e. topographic high point and central lake area) that is flanked by two overdeepened areas (i.e. west and east), the eastern trench dips to the northeast (Lally et al., 2024), whereas the western trench dips to the northwest. The northeastern study area (Lally et al., 2024) is dominated by landforms of glaciofluvial erosion, such as ice-marginal spillways, formed in response to the emerging topography. Jökulsárlón glacial lagoon is first captured in the top right of the May 2022 map, this area of the ice-margin evolves into a lake-terminating section of Esjufjallajökull in the May 2023 map. The western overdeepened area dips to the northwest (Lally et al., 2023) and is characterised by an emerging bedrock ridge, proglacial channels and pitted sandar (Figure 9). The pitted foreland in the west likely formed as the glacier retreated across an overdeepening and meltwater drained via subglacial and englacial sources, remobilising and depositing sediment which buried the snout. This results in large swaths of stagnant ice that will subsequently undergo secondary deglaciation (Everest & Bradwell, 2003), along with the continual evolution of the overlying glaciofluvial outwash deposits. The time-series captures the pitted sandar becoming more complex overtime, with esker ridges emerging (Schomacker et al., 2014; Storrar et al., 2015).

Recessional moraines appear to be absent from the time-series, suggesting that this section of Breiðamerkurjökull is no longer an 'active' temperate glacier, as it does not advance during the winter months (Evans, 2003). Since the late nineties, the warming climate resulted in rapid ice margin retreat (Guðmundsson & Evans, 2022) and such landforms representing periods of stability appear to be absent. As the glacier thins, topography and meltwater processes appear to exert more control on the geomorphic evolution. Meltwater eroded spillways provide evidence for preferential flow of water to topographic lows. Hummocky corridors, including possible murtoo-like forms, potentially provide the first contemporary analogues for similar landforms recently discovered at the ice sheet scale (Ahokangas et al., 2021; Dewald et al., 2021; Ojala et al., 2019, 2021; Peterson et al., 2017; Vérité et al., 2023). While further work is required, their spatial distribution within the time-series could indicate levels of subglacial meltwater at the ice-bed interface and represent a transition zone between an inefficient to efficient drainage system.

Improving our understanding of glacial landforms like hummocky meltwater tracts and geometric ridges is an area of ongoing research (e.g. Evans et al., 2022; Lewington et al., 2019; Peterson & Johnson, 2018; Peterson Becher & Johnson, 2021; Vérité et al., 2022) but the maps provide new insights into the evolution of ice and meltwater dynamics across both space and time at Esjufjallajökull. The detailed database of mapped features can be used as a baseline for subsequent monitoring of (a) ice retreat, (b) landform development, (c) secondary deglaciation of buried ice environments and (d) evolving ice and meltwater dynamics, providing further insights into active processes and proglacial landscape evolution during deglaciation. This aids our interpretation of ice sheet scale deglacial landscapes formed during past glaciations.

Software

UAV data were processed using Agisoft Metashape Professional (v1.8.1) photogrammetry software. All feature digitisation and final map production was completed using ArcGIS Pro (v.3.1.1.). Additional map figures produced for the manuscript were also created in ArcGIS Pro and edited using Inkscape (v.1.3.2), an open-source vector graphics software. All software was supplied under Queen's University Belfast licences.

Acknowledgements

AL was funded by UKRI QUADRAT Doctoral Training Programme (DTP) studentship (NE/S007377/1). AMWN was funded by British Society for Geomorphology Early Career Researcher fund and RDS received funding from the Quaternary Research Association. We would like to especially thank Sigurður Óskar Jónsson of Vatnajökull National Park for supplying us with site advice and research permits. We wish to thank the reviewers, Luis Tanarro, Elina Ahokangas and Ben Stoker for their constructive

feedback, which improved the quality of the final maps and manuscript.

Data availability statement

Data contained within the map series are available upon request.

Disclosure statement

No potential conflict of interest was reported by the author(s).

Funding

This research was supported by UKRI-funded QUADRAT DTP under grant NE/S007377/1, British Society for Geomorphology and Quaternary Research Association.

ORCID

Amy Lally http://orcid.org/0000-0002-3406-0920
Alastair Ruffell http://orcid.org/0000-0001-6072-501X
Andrew Newton http://orcid.org/0000-0002-0089-525X

References

Aðalgeirsdóttir, G., Magnússon, E., Pálsson, F., Thorsteinsson, T., Belart, J. M. C., Jóhannesson, T., Hannesdóttir, H., Sigurðsson, O., Einarssong, B., Berthier, E., Schmidt, L. S., Haraldsson, H., & Björnsson, H. (2020). Glacier changes in Iceland from ~1890 to 2019. *Frontiers in Earth Science, 8*, 1–15. https://doi.org/10.3389/feart.2020.523646

Ahokangas, E., Ojala, A. E. K., Tuunainen, A., Valkama, M., Palmu, J. P., Kajuutti, K., & Mäkinen, J. (2021). The distribution of glacial meltwater routes and associated murtoo fields in Finland. *Geomorphology*, *389*, 107854. https://doi.org/10.1016/j.geomorph.2021.107854

Banerjee, I., & McDonald, B. C. (1975). Nature of esker sedimentation. In A. V. Jopling, & B. C. McDonald (Eds.), *Glaciofluvial and glaciolacustrine sedimentation* (pp. 132–154). SEPM Society for Sedimentary Geology. https://doi.org/10.2110/pec.75.23.0132

Benediktsson, ÍÖ., Aradóttir, N., Ingólfsson, Ó., & Brynjólfsson, S. (2022). Cross-cutting palaeo-ice streams in NE-Iceland reveal shifting Iceland Ice sheet dynamics. *Geomorphology*, *396*, 108009. https://doi.org/10.1016/j.geomorph.2021.108009

Benn, D. I. (1995). Fabric signature of subglacial till deformation, Breiðamerkurjökull, Iceland. *Sedimentology*, *42*(5), 735–747. https://doi.org/10.1111/j.1365-3091.1995.tb00406.x

Bennett, G. L., & Evans, D. J. A. (2012). Glacier retreat and landform production on an overdeepened glacier foreland: The debris-charged glacial landsystem at Kvíárjökull, Iceland. *Earth Surface Processes and Landforms*, *37*(15), 1584–1602. https://doi.org/10.1002/ESP.3259

Bhardwaj, A., Sam, L., Bhardwaj, A., Martín-Torres, F. J., & Kumar, R. (2016). UAVs as remote sensing platform in glaciology: Present applications and future prospects. *Remote Sensing of Environment*, *175*, 196–204. https://doi.org/10.1016/j.rse.2015.12.029

Björnsson, H. (1996). 300 m deep trench created beneath Breiðamerkurjökull during the Little Ice Age. *Annals of Glaciology*, *111*, 141–146. https://doi.org/10.3189/1996AoG22-1-141-146

Boulton, G. S. (1976). The origin of glacially fluted surfaces-observations and theory. *Journal of Glaciology*, *17*(76), 287–309. https://doi.org/10.3189/s0022143000013605

Boulton, G. S. (1986). Push-moraines and glacier-contact fans in marine and terrestrial environments. *Sedimentology*. https://doi.org/10.1111/j.1365-3091.1986.tb01969.x

Boulton, G. S., Dobbie, K., & Zatsepin, S. (2001). Sediment deformation beneath glaciers and its coupling to the subglacial hydraulic system. *Quaternary International*, *86*(1), 3–28. https://doi.org/10.1016/S1040-6182(01)00048-9

Boulton, G. S., Lunn, R., Vidstrand, P., & Zatsepin, S. (2007a). Subglacial drainage by groundwater-channel coupling, and the origin of esker systems: Part 1-glaciological observations. *Quaternary Science Reviews*, *26*(7–8), 1067–1090. https://doi.org/10.1016/j.quascirev.2007.01.007

Boulton, G. S., Lunn, R., Vidstrand, P., & Zatsepin, S. (2007b). Subglacial drainage by groundwater-channel coupling, and the origin of esker systems: Part II-theory and simulation of a modern system. *Quaternary Science Reviews*, *26*(7-8), 1091–1105. https://doi.org/10.1016/j.quascirev.2007.01.006

Bradwell, T., Sigurdsson, O., & Everest, J. (2013). Recent, very rapid retreat of a temperate glacier in SE Iceland. *Boreas*, *42*, 958–973. https://doi.org/10.1111/bor.12014

Chandler, B. M. P., Lovell, H., Boston, C. M., Lukas, S., Barr, I. D., Benediktsson, Í. Ö., Benn, D. I., Clark, C. D., Darvill, C. M., Evans, D. J. A., Ewertowski, M. W., Loibl, D., Margold, M., Otto, J. C., Roberts, D. H., Stokes, C. R., Storrar, R. D., & Stroeven, A. P. (2018). Glacial geomorphological mapping: A review of approaches and frameworks for best practice. *Earth-Science Reviews*, *185*, 806–846. https://doi.org/10.1016/j.earscirev.2018.07.015

Chandler, B. M. P., Chandler, S. J. P., Evans, D. J. A., Ewertowski, M. W., Lovell, H., Roberts, D. H., Schaefer, M., & Tomczyk, A. M. (2020b). Sub-annual moraine formation at an active temperate Icelandic glacier. *Earth Surface Processes and Landforms*, *45*(7), 1622–1643. https://doi.org/10.1002/esp.4835

Chandler, B. M. P., Evans, D. J. A., Chandler, S. J. P., Ewertowski, M. W., Lovell, H., Roberts, D. H., Schaefer, M., & Tomczyk, A. M. (2020a). The glacial landsystem of Fjallsjökull, Iceland: Spatial and temporal evolution of process-form regimes at an active temperate glacier. *Geomorphology*, *361*, 107192. https://doi.org/10.1016/j.geomorph.2020.107192

Chandler, B. M. P., Evans, D. J. A., Roberts, D. H., Ewertowski, M., & Clayton, A. I. (2016a). Glacial geomorphology of the Skálafellsjökull foreland, Iceland: A case study of 'annual' moraines. *Journal of Maps*, *12*(5), 904–916. https://doi.org/10.1080/17445647.2015.1096216

Chandler, B. M. P., Evans, D. J. A., Roberts, D. H., Ewertowski, M., & Clayton, A. I. (2016b). Glacial geomorphology of the Skálafellsjökull foreland, Iceland: A case study of 'annual' moraines. *Journal of Maps*, *12*(5), 904–916. https://doi.org/10.1080/17445647.2015.1096216

Dewald, N., Lewington, E., Livingstone, S. J., Clark, C. D., & Storrar, R. D. (2021). Distribution, characteristics and formation of Esker enlargements. *Geomorphology*, *2*(1), 1–17. https://doi.org/10.1016/j.bcra.2021.100010

Evans, D. J. A. (2003). *Glacial Landsystems*. Arnold.

Evans, D. J. A. (2011). Glacial landsystems of Satujökull, Iceland: A modern analogue for glacial landsystem overprinting by mountain icecaps. *Geomorphology*, *129*, 225–237. https://doi.org/10.1016/j.geomorph.2011.01.025

Evans, D. J. A., Ewertowski, M., & Orton, C. (2016a). Fláajökull (north lobe), Iceland: Active temperate piedmont lobe glacial landsystem. *Journal of Maps*, *12*(5), 777–789. https://doi.org/10.1080/17445647.2015.1073185

Evans, D. J. A., Ewertowski, M., & Orton, C. (2016b). Eiríksjökull plateau icefield landsystem, Iceland. *Journal of Maps*, *12*, 747–756. https://doi.org/10.1080/17445647.2015.1072448

Evans, D. J. A., Ewertowski, M., & Orton, C. (2017a). Skaftafellsjökull, Iceland: Glacial geomorphology recording glacier recession since the Little Ice Age. *Journal of Maps*, *13*(2), 358–368. https://doi.org/10.1080/17445647.2017.1310676

Evans, D. J. A., Ewertowski, M., & Orton, C. (2017b). The glaciated valley landsystem of Morsárjökull, Southeast Iceland. *Journal of Maps*, *13*(2), 909–920. https://doi.org/10.1080/17445647.2017.1401491

Evans, J. A., Ewertowski, M., & Orton, C. (2017c). Skaftafellsjökull, Iceland: Glacial geomorphology recording glacier recession since the Little Ice Age. *Journal of Maps*, *13*(2), 358–368. https://doi.org/10.1080/17445647.2017.1310676

Evans, D. J. A., Ewertowski, M., Orton, C., & Graham, D. J. (2018). The glacial geomorphology of the ice cap piedmont lobe landsystem of east mýrdalsjökull, Iceland. *Geosciences (Switzerland)*, *8*(6), 1–35. https://doi.org/10.3390/geosciences8060194

Evans, D. J. A., Ewertowski, M., Roberts, D. H., & Tomczyk, A. M. (2022). The historical emergence of a geometric and sinuous ridge network at the Hørbyebreen polythermal glacier snout, Svalbard and its use in the interpretation of ancient glacial landforms. *Geomorphology*, *406*, 108213. https://doi.org/10.1016/j.geomorph.2022.108213

Evans, D. J. A., Ewertowski, M. W., Tomczyk, A., & Chandler, B. M. P. (2023). Active temperate glacial landsystem evolution in association with outwash head/depositional overdeepenings. *Earth Surface Processes and Landforms*, *48*(8), 1573–1598. https://doi.org/10.1002/esp.5569

Evans, D. J. A., Nelson, C. D., & Webb, C. (2010a). An assessment of fluting and 'till esker' formation on the foreland of Sandfellsjökull, Iceland. *Geomorphology*, *114*(3), 453–465. https://doi.org/10.1016/j.geomorph.2009.08.016

Evans, D. J. A., & Twigg, D. R. (2000). Breiðamerkurjökull 1998. 1:30,000 Scale Map. University of Glasgow and Loughborough University.

Evans, D. J. A., & Twigg, D. R. (2002). The active temperate glacial landsystem: A model based on Breiðamerkurjökull and Fjallsjökull, Iceland. *Quaternary Science Reviews*, *21*(20-22), 2143–2177. https://doi.org/10.1016/S0277-3791(02)00019-7

Evans, D. J. A., Twigg, D. R., & Orton, C. (2010b). Satujökull glacial landsystem, Iceland. *Journal of Maps*, *6*(1), 639–650. https://doi.org/10.4113/jom.2010.1129

Everest, J., & Bradwell, T. (2003). Buried glacier ice in southern Iceland and its wider significance. *Geomorphology*, *52*, 347–358. https://doi.org/10.1016/S0169-555X(02)00277-5

Everest, J., Bradwell, T., Jones, L., & Hughes, L. (2017). The geomorphology of svínafellsjökull and virkisjökull-falljökull glacier forelands, Southeast Iceland. *Journal of Maps*, *13*(2), 936–945. https://doi.org/10.1080/17445647.2017.1407272

Guðmundsson, S., Björnsson, H., & Pálsson, F. (2017). Changes of Breiðamerkurjökull glacier, SE-Iceland, from its late nineteenth century maximum to the present. *Geografiska Annaler: Series A, Physical Geography*, *99*(4), 338–352. https://doi.org/10.1080/04353676.2017.1355216

Guðmundsson, S., & Evans, D. J. A. (2022). Geomorphological map of Breiðamerkursandur 2018: the historical evolution of an active temperate glacier foreland. *Geografiska Annaler: Series A, Physical Geography*, *104*(4), 298–332. https://doi.org/10.1080/04353676.2022.2148083

Hackney, C., & Clayton, A. I. (2015). Unmanned Aerial Vehicles (UAVs) and their application in geomorphic mapping. *British Society for Geomorphology Geomorphological Techniques*, *2*(17), 1–12.

Howarth, P. J. (1971). Investigations of Two Eskers at Eastern Breiðamerkurjökull, Iceland. *Arctic and Alpine Research*, *3*(4), 305–318. https://doi.org/10.2307/1550046

Howarth, P. J., & Price, R. J. (1969). The proglacial lakes of Breiðamerkurjökull and Fjallsjökull, Iceland. *Geographical Journal*, *135*(4), 573–581. https://doi.org/10.2307/1795105

Howarth, P. J., & Welch, R. (1969a). Breiðamerkurjökull, South-east Iceland, August 1945. 1:30,000 scale map. University of Glasgow.

Howarth, P. J., & Welch, R. (1969b). Breiðamerkurjökull, South-east Iceland, August 1965. 1:30,000 scale map. University of Glasgow.

Jónsson, S. A., Schomacker, A., Benediktsson, ÍÖ, Ingólfsson, Ó, & Johnson, M. D. (2014). The drumlin field and the geomorphology of the Múlajökull surge-type glacier, central Iceland. *Geomorphology*, *207*, 213–220. https://doi.org/10.1016/J.GEOMORPH.2013.11.007

Lally, A., Ruffell, A., Newton, A. M. W., Rea, B. R., Kahlert, T., Storrar, R. D., Spagnolo, M., Graham, C., & Coleman, M. (2023). The evolution and preservation potential of englacial eskers: An example from Breiðamerkurjökull, SE Iceland. *Earth Surface Processes and Landforms*, *48*(14), 2864–2883. https://doi.org/10.1002/esp.5664

Lally, A., Ruffell, A., Newton, A. M. W., Rea, B. R., Spagnolo, M., Storrar, R. D., Kahlert, T., & Graham, C. (2024). Geomorphological signature of topographically controlled ice flow-switching at a glacier margin: Breiðamerkurjökull (Iceland) as a modern analogue for palaeo-ice sheets. *Geomorphology*, *454*, 109184. https://doi.org/10.1016/j.geomorph.2024.109184

Leigh, J. R., Evans, D. J. A., Stokes, C. R., Andreassen, L. M., & Carr, R. J. (2021). Glacial and periglacial geomorphology of central Troms and Finnmark county, Arctic Norway. *Journal of Maps*, *17*(2), 348–366. https://doi.org/10.1080/17445647.2021.1950580

Lewington, E. L. M., Livingstone, S. J., Sole, A. J., Clark, C. D., & Ng, F. S. L. (2019). An automated method for mapping geomorphological expressions of former subglacial meltwater pathways (hummock corridors) from high resolution digital elevation data. *Geomorphology*, *339*, 70–86. https://doi.org/10.1016/j.geomorph.2019.04.013

Lister, H. (1951). Report on glaciology at Breiðamerkurjökull 1951. *Jokull*, *3*(1), 23–31.

Öhrling, C., Peterson, G., & Johnson, M. D. (2020). Glacial geomorphology between Lake Vänern and Lake Vättern, southern Sweden. *Journal of Maps*, *16*, 776–789. https://doi.org/10.1080/17445647.2020.1820386

Ojala, A. E. K., Mäkinen, J., Ahokangas, E., Kajuutti, K., Valkama, M., Tuunainen, A., & Palmu, J. P. (2021). Diversity of murtoos and murtoo-related subglacial

landforms in the Finnish area of the Fennoscandian Ice Sheet. *Boreas*, *50*, 1095–1115. https://doi.org/10.1111/bor.12526

Ojala, A. E. K., Peterson, G., Mäkinen, J., Johnson, M. D., Kajuutti, K., Palmu, J. P., Ahokangas, E., & Öhrling, C. (2019). Ice-sheet scale distribution and morphometry of triangular-shaped hummocks (murtoos): A subglacial landform produced during rapid retreat of the Scandinavian Ice Sheet. *Annals of Glaciology*, *60*(80), 115–126. https://doi.org/10.1017/aog.2019.34

Peterson, G., & Johnson, M. D. (2018). Hummock corridors in the south-central sector of the Fennoscandian ice sheet, morphometry and pattern. *Earth Surface Processes and Landforms*, *43*, 919–929. https://doi.org/10.1002/esp.4294

Peterson, G., Johnson, M. D., & Smith, C. A. (2017). Glacial geomorphology of the south Swedish uplands – focus on the spatial distribution of hummock tracts. *Journal of Maps*, *13*, 534–544. https://doi.org/10.1080/17445647.2017.1336121

Peterson Becher, G., & Johnson, M. D. (2021). Sedimentology and internal structure of murtoos – V-shaped landforms indicative of a dynamic subglacial hydrological system. *Geomorphology*, *380*, 1–16. https://doi.org/10.1016/j.geomorph.2021.107644

Price, R. J. (1969). Moraines, Sandar, Kames and Eskers near Breiðamerkurjökull, Iceland. *Transactions of the Institute of British Geographers* 46: 17–43. https://doi.org/10.2307/621406

Price, R. J. (1971). The development and destruction of a sandur, Breiðamerkurjökull, Iceland. *Arctic and Alpine Research*, *3*(3), 225–237.

Price, R.J. (1973). *Glacial and fluvioglacial landforms*. Longman.

Price, R. J. (1982). Changes in the proglacial area of Breiðamerkurjökull, southeastern Iceland: 1890–1980. *Jökull*, *32*, 29–35. https://doi.org/10.33799/jokull1982.32.029

Price, R. J., & Howarth, P. J. (1970). The evolution of the drainage system (1904–1965) in front of Breiðamerkurjökull, Iceland. *Jökull*, *20*, 27–37. https://doi.org/10.33799/jokull1970.20.027

Ramsankaran, R., Navinkumar, P. J., Dashora, A., & Kulkarni, A. (2020). UAV-based Survey of Glaciers in Himalayas: Opportunities and Challenges. https://doi.org/10.20944/preprints202002.0442.v1

Rodríguez-Mena, M., Fernández-Fernández, J. M., Tanarro, L. M., Zamorano, J. J., & Palacios, D. (2021). Héðinsdalsjökull, northern Iceland: geomorphology recording the recent complex evolution of a glacier. *Journal of Maps*, *17*, 301–313. https://doi.org/10.1080/17445647.2021.1920056

Schomacker, A., Benediktsson, ÍÖ, & Ingólfsson, Ó. (2014). The Eyjabakkajökull glacial landsystem, Iceland: Geomorphic impact of multiple surges. *Geomorphology*, *218*, 98–107. https://doi.org/10.1016/J.GEOMORPH.2013.07.005

Sigbjarnarson, G. (1970). On the recession of Vatnajokull. *Jökull* 20: 50–61. https://doi.org/10.33799/jokull1970.20.050

Sigurdsson, O., Jónsson, T., & Jóhannesson, T. (2007). Relation between glacier-termini variations and summer temperature in Iceland since 1930. *Annals of Glaciology*, *46*, 170–176. https://doi.org/10.3189/172756407782871611

Śledź, S., Ewertowski, M. W., & Evans, D. J. A. (2023). Quantification of short-term transformations of proglacial landforms in a temperate, debris-charged glacial landsystem, Kviárjökull, Iceland. *Land Degradation and Development*, *34*, 5566–5590. https://doi.org/10.1002/ldr.4865

Śledź, S., Ewertowski, M., & Piekarczyk, J. (2021). Applications of unmanned aerial vehicle (UAV) surveys and Structure from Motion photogrammetry in glacial and periglacial geomorphology. *Geomorphology*, *378*, 107620. https://doi.org/10.1016/j.geomorph.2021.107620

Storrar, R. D., Evans, D. J. A., Stokes, C. R., & Ewertowski, M. (2015). Controls on the location, morphology and evolution of complex esker systems at decadal timescales, Breiðamerkurjökull, southeast Iceland. *Earth Surface Processes and Landforms*, *40*(11), 1421–1438. https://doi.org/10.1002/esp.3725

Tweed, F. S., Roberts, M. J., & Russell, A. J. (2005). Hydrologic monitoring of supercooled meltwater from Icelandic glaciers. *Quaternary Science Reviews*, *24*, 2308–2318. https://doi.org/10.1016/j.quascirev.2004.11.020

Vérité, J., Ravier, É, Bourgeois, O., Bessin, P., Livingstone, S. J., Clark, C. D., Pochat, S., & Mourgues, R. (2022). Formation of murtoos by repeated flooding of ribbed bedforms along subglacial meltwater corridors. *Geomorphology*, *408*, 108248. https://doi.org/10.1016/j.geomorph.2022.108248

Vérité, J., Ravier, É, Bourgeois, O., Bessin, P., & Pochat, S. (2023). New metrics reveal the evolutionary continuum behind the morphological diversity of subglacial bedforms. *Geomorphology*, *427*, 108627. https://doi.org/10.1016/j.geomorph.2023.108627

Welch, R., & Howarth, P. J. (1968). Photogrammetric measurements of glacial landforms. *Photogrammetric Record*, *6*(31), 75–96. https://doi.org/10.1111/j.1477-9730.1968.tb00915.x

Westoby, M. J., Brasington, J., Glasser, N. F., Hambrey, M. J., & Reynolds, J. M. (2012). Structure-from-Motion' photogrammetry: A low-cost, effective tool for geoscience applications. *Geomorphology*, *179*, 300–314. https://doi.org/10.1016/j.geomorph.2012.08.021